Nano Energy 68 (2020) 104385

Contents lists available at ScienceDirect

Nano Energy

journal homepage: http://www.elsevier.com/locate/nanoen

Communication

Exploring interface confined water flow and evaporation enables solar-thermal-electro integration towards clean water and electricity harvest via asymmetric functionalization strategy

Peng Xiao [a,b], Jiang He [a,b], Feng Ni [a,b], Chang Zhang [a], Yun Liang [a,b], Wei Zhou [a,b], Jincui Gu [a], Junyuan Xia [a], Shiao-Wei Kuo [c], Tao Chen [a,b,*]

[a] Key Laboratory of Marine Materials and Related Technologies, Zhejiang Key Laboratory of Marine Materials and Protective Technologies, Ningbo Institute of Material Technology and Engineering, Chinese Academy of Sciences, Zhongguan West Road 1219, 315201, Ningbo, China
[b] School of Chemical Sciences, University of Chinese Academy of Science, Beijing, 100049, China
[c] Department of Material and Optoelectronic Science, Center of Crystal Research, National Sun Yat-Sen University, 804, Kaohsiung, Taiwan

ARTICLE INFO

Keywords:
Asymmetric functionalization
Solar-thermal-electro conversion
Water flow
Water evaporation
Clean water and power production

ABSTRACT

Water evaporation is a ubiquitous phenomenon in nature. To fully explore the solar-enabled water evaporation can effectively alleviate the growing concern of shortage of water and also energy source. Although significant advances have been achieved for alternative combination of multifunctional applications to explore the unexploited or wasted thermal/solar energy. However, it remains a great challenge for an effective integration of desired functions into one photo-thermal material for extensive harvesting solar energy. Herein, interfacial confined water flow and evaporation are rationally explored to realize an efficient combination of solar-heating enhanced water-flow-induced power generation and interfacial water evaporation. The effective solar-thermal-electro integration is enabled by one multifunctional Janus material via an asymmetric functionalization strategy. As a proof-of-concept, a bilayer carbon nanotubes (CNTs) film/cellulose paper is employed to function as an efficient solar-driven evaporator. Moreover, the as-prepared CNTs-based paper can be further asymmetrically decorated with hydrophobic polydimethylsiloxane (PDMS) and utilized to collect electricity from the directional water flow under dark and light condition. The monolithic design concept is expected to effectively utilize the water evaporation process for integrated electricity and clean water generation.

1. Introduction

Water cycle is an indispensable and ubiquitous process in nature, which is generally constituted of water flow, evaporation and condensation. In this process, effective solar irradiation can further boost the evaporation or transpiration behaviors for enhanced fresh water regeneration to fulfil essential survivals of living creatures. To highly convert solar energy into available resources is of great significance to create a sustainable future for the earth. Nowadays, with the explosive development of human society, growing concern of heavy consumption of fresh water and also energy source has aroused extensive interests in the field of renewable and sustainable energy technologies [1–9]. Solar energy that features in green and renewable property is considered as an inexhaustible resource to alleviate the shortage of energy and clean water sources [10,11]. In recent years, a variety of solar-based exploitation is highly devoted to realize photovoltaic energy conversion and storage [12–14], photo-catalysis [15,16], photo-thermal conversion [6,17–19], *etc*. Specifically, solar-to-thermal techniques target at simple and direct strategies to harvest solar energy for high-efficient water purification [20–25], sterilization [26] and thermoelectricity [27,28]. As a newly emerging member, solar-driven water evaporation that focuses on local heating at water-air interface is highly promising for high-efficient clean water production [18,29–31]. Over the past few years, extensive efforts have been dedicated to developing sunlight absorbers materials, such as plasmonic metal particles [20,22], carbon-based nanostructures [21,32–35], bilayer wood absorbers [36–38], graphene aerogels [25,36], hierarchically nanostructured gels [39], *etc*. Also, the exploration of alternative combination of

* Corresponding author. Key Laboratory of Marine Materials and Related Technologies, Zhejiang Key Laboratory of Marine Materials and Protective Technologies, Ningbo Institute of Material Technology and Engineering, Chinese Academy of Sciences, Zhongguan West Road 1219, 315201, Ningbo, China.
E-mail address: tao.chen@nimte.ac.cn (T. Chen).

https://doi.org/10.1016/j.nanoen.2019.104385
Received 12 October 2019; Received in revised form 15 November 2019; Accepted 5 December 2019
Available online 7 December 2019

thermoelectric materials, salinity gradient power generation or other potential technologies into solar absorbers system has provided an effective pathway for synergic utilization of solar energy [40–44]. However, in some cases, the current multifunctional devices are usually composed of non-integrated functional materials system or non-flexible structural composition, which may have negative effects in low environmental adaptability. For instance, the additional thermoelectric devices can remarkably increase the expenses and the rigid structural facilities may weaken the portability and operability.

Water evaporation is a common phenomenon, which usually occurs at water-air interface. Specifically, interfacial confined water evaporation that involved in the water-permeable solid materials contains two processes, including the capillarity induced water flow to the materials surface and the process of heating water to steam. Moreover, the solar-enhanced water evaporation can further promote the water flow process. As a newly-developed green energy, the evaporation-driven water flow process that harvests thermal energy from the surrounding environment can realize efficient power production [1,45]. Note that the directional protons flow is highly crucial to produce electricity, in which the transport pathway of water molecules should be well-established [46–48]. Since inhomogeneous functional groups distribution of structural materials (e.g. porous carbon membranes [1,49], graphene oxide (GO) films [50,51], *etc.*) or moisture gradient [52,53] from the environments can both trigger the formation of water flow gradient, the power generator can continue to work without additional external stimuli. This novel approach has provided a powerful pathway to achieve continuous electricity harvesting. As a result, full exploration of the process of water flow and evaporation within one integrated functional material is considered to be an alternative and promising approach for realization of high-efficient solar-thermal-electro conversion [54].

In this work, inspired by the process of water evaporation, we demonstrate a concept of synergetic integration of water evaporation and power generation into one asymmetrically functionalized hybrid composed of carbon nanotubes (CNTs), cellulose paper and polydimethylsiloxane (PDMS). In our system, a large-area CNTs film was self-assembled at air/water interface via Marangoni effect and capillary force driven compression strategy [55–60]. The achieved film was further transferred onto the surface of paper for a bilayer solar evaporator [61]. In order to realize a controllable water flow channel, it was further asymmetrically modified with hydrophobic PDMS on the specific location of the paper side. As a result, a centimeter-sized water path can be achieved, which can efficiently drive the directional water flow for efficient electricity generation with/without solar illumination [1]. Significantly, the output power can also be prominently enhanced under solar irradiation. The considerable exploitation of the evaporation process has demonstrated potential advantage for the development of solar-thermal-electro system.

2. Experimental section

2.1. Materials

The raw carbon nanotubes (CNTs) (length, about 10–30 μm; diameter, about 10–30 nm; –COOH %, about 1.5 wt%) with a purity of over 90% were acquired from Chengdu Organic Chemistry Co., Ltd., and were rinsed thoroughly with anhydrous ethanol and dried in a stream of nitrogen before use. General chemicals in chemical reagent grade were used as received from Sinopharm Chemical Reagent.

2.2. Formation of CNTs film

The CNTs powders were firstly dispersed in anhydrous ethanol solution, followed by strong ultrasonication for at least 5 h to form a stable dispersion with appropriate aging time. The as-prepared suspensions spread onto the water surface by spray-coating method for appropriate volume, resulting in uniform preassembled film formed at air/water interface. Subsequently, a porous sponge was used to put on one side of the interface to quickly siphon water from the system. Notably, the homogenous preassembled film was closely packed towards the opposite direction of the syphone direction. When the area of the film was not further decreased, the resulted film was ultimately formed, indicating a closely packed structure.

2.3. Fabrication of CNTs/paper

A commercial Xerox paper was gently attached onto the air side of the CNTs film at air/water interface. Owing to the strong capillary force of the fibrous paper, water molecules can be absorbed into the paper through the porous network of the CNTs film. Since the paper was thoroughly wetted, it could spread smoothly on the water surface, demonstrating a successful transfer of the CNTs film. The resulted CNTs/paper can be directly peeled from the water surface, followed by a rigorous rinsing procedure using the deionized water. After drying process, the CNTs/paper was further treated with oxygen plasma to acquire a hydrophilic surface for continuous water transportation.

Preparation of CPPH: Sylgard 184 (the ratio between component A and B was 1:10) solution was dropped onto specific part of the paper side of the as-prepared CNTs/paper film followed by a typical PDMS curing process (at 70 °C for 2 h). Specifically, to effectively avoid the undesirable PDMS penetration into the CNTs network, the CNTs film was previously wetted with water. Owing to the incompatibility between water and hydrophobic PDMS, the PDMS polymer can be efficiently confined to the paper substrate. As a result, an asymmetrically structured hybrid was achieved. Specifically, in order to realize a self-floating behavior, the edge of resulted CPPH was encapsulated with hydrophobic PDMS.

2.4. Solar vaporization experiments

Square CNTs/paper samples (9 mm in diameter) with different CNTs film thickness and CPPH samples were floated on water surface in a plastic tube, which were irradiated by a solar simulator equipped with AM 1.5G. The mass changes were measured for 60 min at constant condition.

2.5. Electricity generation experiments

CNTs film on the PDMS-modified paper was decorated with commercially available conductive fabric composed of Ni, Cu and polyethylene terephthalate (PET) for an electrode, which was subsequently encapsulated with PDMS. A conductive carbon fiber was put into the water or simulated seawater (3.5 wt%). The conductive fabric and the carbon fiber were connected with the detector to measure the generated voltage and current, individually.

2.6. Characterization

Field Emission Scanning Electron Microscope (FE-SEM) images were obtained with a FE scanning electron microanalyzer (Hitachi-S4800, 4 kV). The CNTs/paper has experienced a hydrophilic treatment using oxygen plasma for 80 s in a plasma cleaner (Tonson Tech TS-P05, 40 KHz, power 200 W). Optical Transmittance of the films was probed using UV–vis–NIR spectra, which were obtained with a Lambda 950 spectrophotometer from PerkinElmer Instrument Co., Ltd. USA. IR camera (Optris PI400) with a resolution of 382 × 288 pixels was adopted to record the surface temperature of the CNTs/paper and CPPH samples. The data was analyzed by the PI connect software. Solar simulator (HM-Xe500W) was employed as the light resource in lab, which was equipped with standard AM 1.5 G solar irradiance density spectrum. The water evaporation rate was accurately measured by using an electronic scale (GXG-JJ224BC). The current and voltage changes for power suppliers were recorded by CHI660E electrochemical system, digit multimeter

(Keysight 34461A) and a semiconductor parameter analyzer (Keithley 4200).

3. Results and discussion

The schematic fabrication procedures of CNTs/PDMS/paper hybrid (hereby designated as CPPH) is illustrated in Fig. 1a, in which the CNTs film at air/water interface was *in situ* transferred onto one side of the Xerox paper. Following a typical drying process, part of the paper side of the resulted CNTs/paper was further asymmetrically modified by hydrophobic PDMS layer, aiming to prevent water permeation from the bulk water. To ensure a controllable water pathway and self-floating behavior, the edge of the CPPH was tightly encapsulated by PDMS (Fig. S1). Due to the hydrophobic property of PDMS with low surface tension, the achieved CPPH can stably float on the surface of water or simulated seawater. Once the CPPH was put on the water surface, water molecules can be pumped into the CNTs network surface via capillary force for continuous water evaporation under solar illumination. Furthermore, the well-designed asymmetric structure can significantly induce the water flow along specific part of the CPPH, enabling a spontaneous power collection. More importantly, due to the water flow driven electricity generation mechanism, the process can favorably happen with and without sunlight. The *in situ* transfer strategy allowed the formation of uniform CNTs film on the fibrous paper surface (Fig. 1b).

When the hydrophobic PDMS was coated onto paper side of the CNTs/paper, the color of the paper could experience a remarkable change from white to black, in which the color of CNTs film in the opposite side can be highly reflected. This phenomenon may derive from the difference of refractive index before and after PDMS coating. Generally, the gaps among cellulose fibers are filled with air and the corresponding refractive index of air is about 1. However, the PDMS coating with refractive index of about 1.41 can remarkably change the light pathway, which can experience multiple refraction and reflection process. As a result, the incident light may pass through the cellulose paper for enhanced transmittance, endowing the black CNTs film on the opposite side with desirable visibility (Fig. S2). As displayed in Fig. 1c, the PDMS-modified part could be clearly observed with the naked eyes. Owing to the favorable photo-thermal feature of the CPPH, it was further employed as the solar evaporator, demonstrating reliable water evaporation performance even under high solar intensity of 5 kW/m^2 (Fig. 1d). More interestingly, the CPPH can also function as the power generator driven by the capillarity induced water flow, which can both work with and without sunlight (Fig. 1e) [62]. Microscopically, to further investigate the microstructure of the CPPH, SEM characterization was adopted. As shown in Fig. 1f and e, the interlaced tubular CNTs network on fibrous paper surface can provide a desirable capillary force for effective water absorption. To construct a controllable pathway for directional water flow, the PDMS that penetrated into the paper could effectively prevent the permeation of the water molecules (Fig. 1g). As a result, the water can flow smoothly across the CNTs film surface for efficient electricity generation.

Due the excellent flat and flowable features of the water surface, it is considered as an ideal platform to realize a scalable two-dimensional (2D) film production and subsequent *in situ* transfer onto diverse targets. To form a large-area CNTs film, a sprayer was adopted to spread CNTs dispersion onto water surface induced by Marangoni effect (Fig. S3). After spraying appropriate amount of CNTs dispersion, a uniform preassembled CNTs film could be readily achieved. In order to achieve a close-packed structure, a porous sponge was used to compress the preassembled film to a condensed one (Fig. S3). Even the sponge was removed from the water surface, the formed CNTs film in large scale can still maintain a stable state due to the physical entanglement (Fig. S4a). SEM images were further employed to characterize the surface morphology and thickness of the acquired CNTs film. As shown in Fig. S4b and c, a porous structure with condensed network was clearly observed, in which the capillary force could be ensured to realize a desirable water flow. In addition, the uniform thickness of the CNTs film allows the formation of controllable thickness after multiple transfer of CNTs films (Fig. S4d).

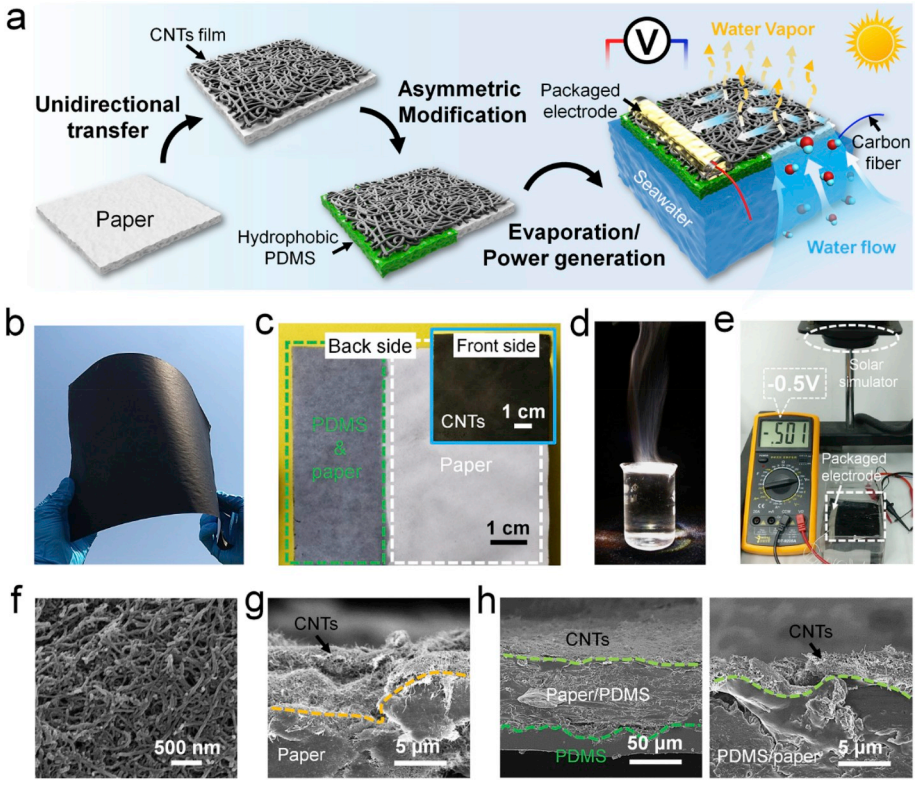

Fig. 1. a) Schematic of fabrication of CPPH for all-in-one evaporator towards simultaneous water evaporation and electricity generation. b) Photograph of uniform CNTs/paper with favorable flexibility. c) Photo of hydrophobic PDMS asymmetrically modified CNTs/paper with apparent edges. d) Photo of abundant steam generated under solar irradiation of 5 kW/m^2 e) The as-prepared CPPH enables the formation of water flow across the CNTs film to realize the power generation. f) SEM image of the solar absorber layer decorated with CNTs film. Cross-section SEM images of g) CNTs/paper and h) PDMS modified CNTs/paper with smooth morphology of PDMS, which can significantly prevent the permeation of water molecules.

To achieve a non-destructive transfer of the resulted CNTs film onto cellulose paper surface, an *in situ* capillarity driven transfer strategy is developed in our system. As schematically displayed in Fig. S5, the cellulose paper was gently and directly put on the air side of the CNTs film. Upon it was contacted with water, the water molecules driven by capillary force within the fibrous structure of paper could penetrate through the porous CNTs film into the paper. Additionally, the capillary force can remarkably enhance the interaction between CNTs film and paper, allowing the formation of tight solid-solid interface (Fig. S5). As shown in Fig. S6a, when the white paper was thoroughly wetted by the water, it could spread flat to the surface of water, which demonstrated a sharp contrast with the original paper. After peeling off from the water surface, a stable CNTs/paper was finally acquired and could endure rigorous washing without apparent delamination (Figs. S6b and S6c). Through this simple and efficient way, a large-scale CNTs/paper was readily achieved, demonstrating good uniformity and flexibility, which can be favorably folded into desired shapes (Fig. 2a). Moreover, this simple and reproducible interfacial transfer manner allows us to acquire well-controlled CNTs layer thickness with repetitive operation. A series of CNTs/paper with controllable thickness ranging from 1 layer to 5 layers can be fabricated. Microscopically, the morphology and cross-section information of as-prepared film was confirmed by SEM images in Fig. 2b. It was observed that with the increase of CNTs film layers, the rough surface of the cellulose paper became much smoother, demonstrating more condensed CNTs network. Specifically, the interfacial transfer approach enables a non-destructive deposition of CNTs film on cellulose paper surface, in which the conductivity of the resulted paper hybrid is competitive to that of the paper formed by conventional transfer strategy from the water phase (Fig. 2c). Furthermore, the conductivity of the CNTs/paper with a series of CNTs layers was also investigated in Fig. 2d, indicating a negative correlation between resistance and CNTs layers.

To investigate the performance of light absorption, optical properties of the CNTs/paper were measured with an ultraviolet visible-near-infrared (UV-VIS-NIR) spectrophotometer. Compared with the original paper, the CNTs/paper demonstrated relatively higher absorption in all spectral ranges. Moreover, to optimize the evaporation performance, different CNTs layer thickness ranging from ~0.6 (1 layer) to ~3 μm (5 layers) was also investigated in our system. With the increase of CNTs load, the absorption of as-prepared film presented a gradual increasing tendency (Fig. 2e). It was found that film with 5 layers can absorb almost 95% of UV, 96% of visible, and 90% of infrared solar irradiation with a total absorption capacity of 93.7% over the whole solar spectrum. To further compare the surface temperature and corresponding distribution of the bilayer CNTs/paper with that of bulk water, 3 layers of CNTs film was adopted to measure the performance difference due to its relatively stable light absorption. Superior to the bulk water with equilibrium temperature of ~24 °C, the bilayer CNTs/paper can experience a

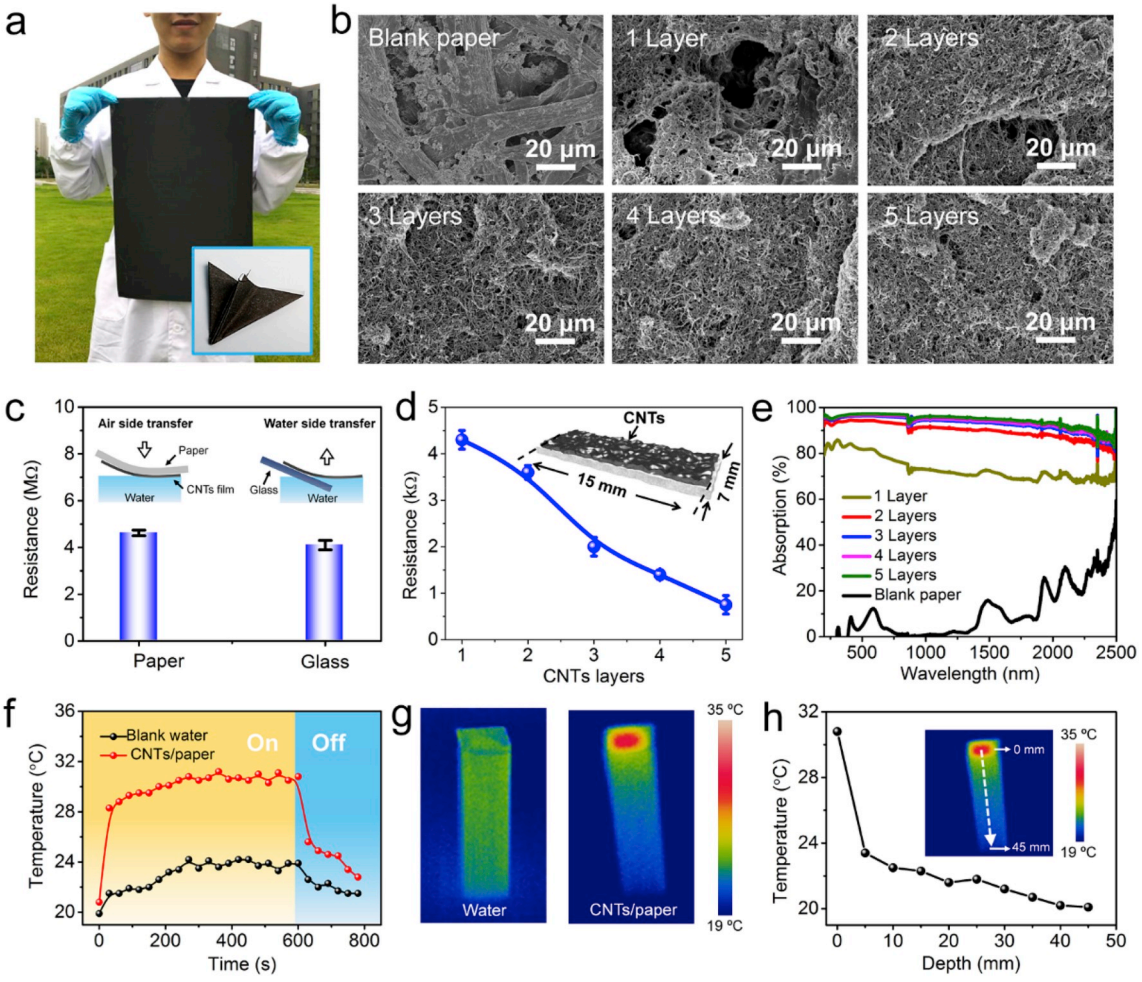

Fig. 2. a) Photo of scalable fabrication of CNTs/paper with desirable foldability through an *in situ* capillary force driven transfer way. b) SEM images of original paper surface and CNTs/paper composite with a series of CNTs layers. c) The resistance comparison of CNTs film on glass substrate and the capillarity driving transfer onto paper surface. d) Resistance versus different CNTs layers on paper substrate curve. e) Light absorption spectra of CNTs/paper film with different CNTs layers. f) Temperature versus time curves of blank water and CNTs/paper. g) IR images of blank water and CNTs/paper on water surface under 1 sun. h) The vertical temperature distribution curve of the CNTs/paper.

remarkable temperature improvement from ~21 °C to ~31 °C under 1 sun within 6 min (Fig. 2f). The bilayer structure of the CNTs/paper could extremely decrease the heat diffusion from the light absorber layer to the water subphase, which was displayed by IR images in Fig. 2g. In addition, the vertical temperature distribution of the CNTs/paper on water surface was also investigated in Fig. 2h, in which the temperature functioned as a negative correlation with depth, indicating that the heat was extremely confined on the CNTs/paper surface.

Significantly, in the bilayer system, the unmodified paper can both act as the water pumping layer and heat isolation layer, which can prominently enhance the photo-thermal conversion in high-efficiency (Fig. 3a). To further explore the water evaporation performance of the CNTs/paper, a series of water evaporation experiments were conducted under solar illumination. The weight changes of bulk water and bilayer CNTs/paper with a series of CNTs film layers over time curves under 1 sun were recorded in Fig. 3b. Superior to blank sample, the CNTs/paper demonstrated higher weight loss. To optimize the evaporation efficiency, the correlation between CNTs film layers and corresponding evaporation rates were also inspected. As shown in Fig. 3c, it was found that with the increase of CNTs load (up to ~3 μm, 5 CNTs film layers), the evaporation rate represented a parabola-like tendency. As a result, CNTs/paper with 3-layer CNTs films demonstrated a higher evaporation rate of about 1.15 kg/m^2. The reason may derive from the competitive balance between light absorption and water pumping. Excess CNTs load could result in smaller capillary pores of the CNTs network, demonstrating a poor water pumping rate from the water subphase. In addition, the amplified SEM characterization of samples with 3, 4, and 5 CNTs layers was conducted in Fig. S7. The result shows that with the increase of CNTs layers, the gaps among the CNTs network have become smaller and smaller. However, the light absorption of the above-mentioned samples can experience a gradual and slight increase process, which can result in improved solar-to-thermal conversion. From Fig. S8 it can be supposed that when CNTs layers (more than 3) increases, the acquired evaporation rate demonstrates a gradual decrease tendency. The negative correlation between light absorption and evaporation rate can indirectly evidence that the smaller pores severely block the water transportation during the solar-driven interfacial water evaporation process. Therefore, 3-layered CNTs load was adopted in our system. The mass change curves under solar intensity from 0.5 to 2.5 sun were recorded in Fig. 3d and the calculated evaporation rate is found to increase linearly with the optical concentration (Fig. 3e).

When hydrophobic PDMS was asymmetrically coated onto CNTs/paper surface, a well-designed water pathway was achieved. As illustrated in Fig. 3f, PDMS-modified side of the CPPH can function as a water-proof layer to prevent any water penetration. As a result, water molecules are merely interfacially confined on the paper side of the CPPH, which can further penetrate into the fibrous paper and move across the CNTs film surface for controllable solar-driven water evaporation. Moreover, IR images were captured to indirectly investigate water flow pathway under 1 sun illumination. As shown in Fig. 3g, the surface temperature distribution of the CPPH was clearly observed. The CNTs film on the PDMS- functionalized paper surface showed higher temperature than that without PDMS modification within 0.5 min. The result strongly evidences that water molecules cannot penetrate into the PDMS-modified paper. With the increase of illumination time, the surface temperature difference of the CPPH was getting smaller and

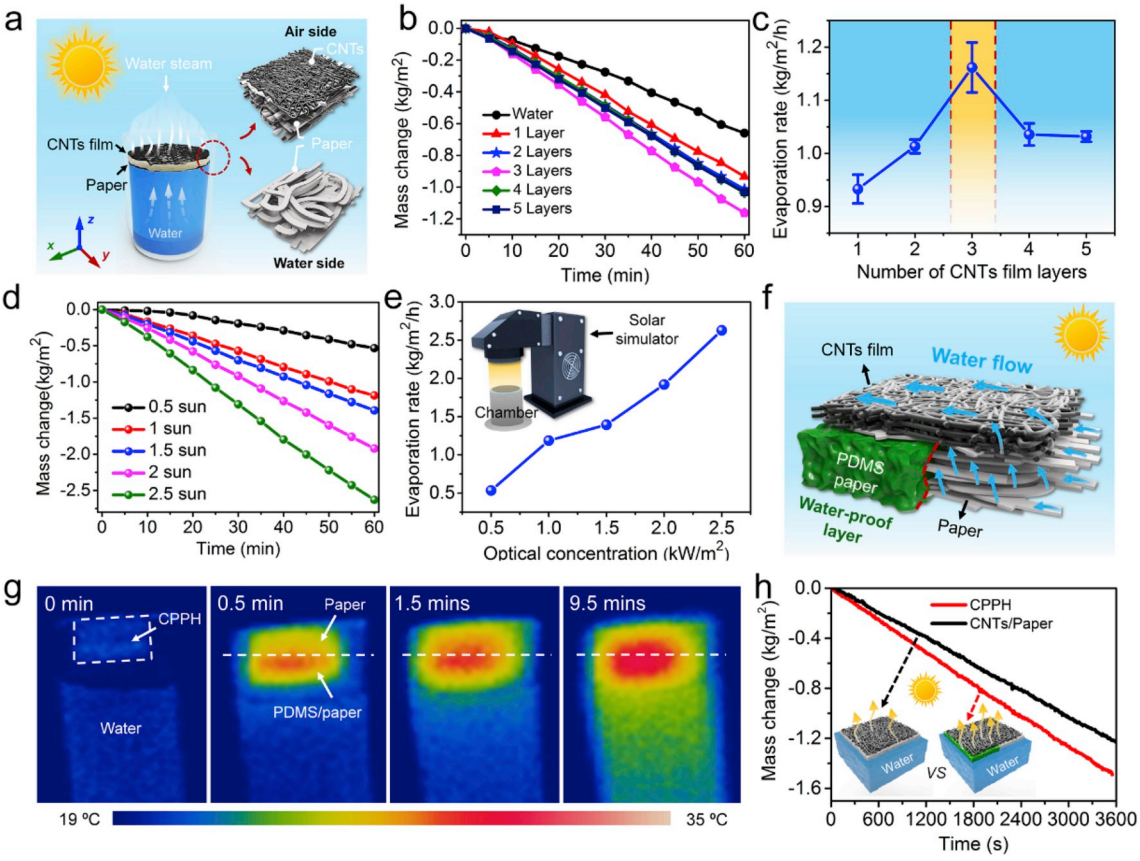

Fig. 3. a) Sketch of the water evaporation of bilayer CNTs/paper at air/water interface under solar irradiation. b) Mass change versus time curves of bulk water and CNTs/paper with different CNTs layers under 1 sun irradiation. c) Evaporation rate versus CNTs film layers curve. d) Mass change over time curves of film with 5-layer CNTs/paper under a series of sun irradiation ranging from 0.5 sun to 2.5 sun. e) The corresponding evaporation rate versus optical concentration curve. f) Sketch of CPPH with designed structure enabling controllable water pathway. g) IR images of CPPH on water surface under 1 sun irradiation. h) Mass change versus time curves of CNTs/paper and CPPH.

smaller. However, contributed to the high water absorption of the CNTs/paper without PDMS modification, the surface temperature of CNTs film was still slightly lower than that of the CNTs/paper with PDMS modification. This phenomenon illustrates that water molecules experience a controllable flow across the CNTs film from paper side to the PDMS-modified paper side. Meanwhile, the control experiment was also conducted to investigate the water evaporation performance of the CNTs/paper with/without PDMS modification. As displayed in Fig. 3h, CPPH sample demonstrated higher water evaporation rate than that of the CNTs/paper sample, which may derive from the relatively high surface temperature of the CPPH. As a result, the evaporation performance of CPPH was not affected by the asymmetric decoration of hydrophobic PDMS.

Furthermore, the outdoor experiments were also conducted to explore the practical performance of water evaporation. As schematically illustrated in Fig. S9a, a well-designed prototype was set up for water distillation. For practical application, a large-scale prototype was fabricated and employed to conduct solar steam generation experiments (Fig. S9b). In a sealed chamber, the vapor was generated from the film surface under solar irradiation and subsequently condensed into liquid when it arrived at the relatively cold condensation roof. Fig. S9c clearly showed that the chamber roof was covered with abundant condensed water droplets, demonstrating an efficient water collection. To explore the practical performance of distillation, two consecutive days that were partly sunny days with roaming cloud (10, 11 September 2017) were selected to collect distilled water (Fig. S9d). Attributed to the cloudy factor, the optical concentration varied dramatically with solar flux ranging from 11 to 830 W/m^2. After distillation, the average evaporate rates were calculated, enabling 3.4 and 5.1 kg/m^2 of purified water in the whole day, which demonstrates a significant potential for efficient water supply in reefs and islands (Fig. S9e).

Since the bilayer CNTs/paper towards the application of interfacial water evaporation is floated on the air-water interface, there is almost no prominent water gradient difference in lateral surface of CNTs film. However, the conventional water flow-induced electricity generation is based on the partial insertion of carbon nanomaterials/glass into water for the formation of water gradient (Fig. S10a). For the realization of simultaneous water evaporation and power production, the partially inserted out-of-plane structure is converted into an in-plane one. In our system, hydrophobic PDMS is applied onto paper surface, which enables the formation of controllable water transportation pathway. The achieved asymmetric structure can realize favorable water gradient, resulting in directional hydrated ions migration (Fig. S10b). To further explore the capability of electricity generation of the CPPH, a conductive fabric electrode was attached onto the CNTs film (3 layers) surface on the PDMS-modified part, which was further encapsulated by PDMS. When the PDMS packaged electrode was applied on the part of CNTs/paper without PDMS modification, unfavorable water wetting phenomenon would happen both in fibrous paper substrate and CNTs film, which can severely break the interaction between CNTs film and electrode. It may result in high contact resistance and undesirable delamination of the applied electrode. Moreover, to avoid the undesirable corrosion or potential electrochemical reaction from the seawater, a commercially available conductive carbon fiber was employed and immersed into simulated seawater to construct a single electrode on CPPH surface as an equivalent circuit. Compared with the reported oxygen plasma-treated candle soot [1], there are relatively low voltage for CPPH using the deionized water, which is also observed in our system. Since the salt solution can remarkably enhance the hydrovoltaic system, the electricity production process can be effectively improved [1].

The detailed electricity generation process is schematically illustrated in Fig. S11, in which the encapsulated electrodes and carbon fiber can achieve a circuit for water flow-induced electricity harvest. Note that the hydrated ions can have a directional migration inside the –COOH groups functionalized CNTs film network for induced voltage and current. Specifically, the interfacial solar heating is achieved by using the seawater to extract desalted water. Therefore, simulated seawater can both act as “precursor” of purified water and “enhancer” of power generator in our system. To investigate the sunlight-enhanced effect on the resulted generating performance, the control experiment was also conducted under the environments with/without sunlight. As schematically illustrated in Fig. 4a, contributed to the alternative modification of PDMS layer, the achieved electricity generator allowed the directional transportation of the water molecules from bulk water to the part of fibrous paper. Subsequently, the plasma-treated CNTs film allows the desirable lateral flow of hydrated ions across the surface of CNTs film, ensuring the directional and continuous protons flow [63]. Once the simulated sunlight was applied on the CPPH-based power generator, the water evaporation rate could be significantly enhanced under solar illumination, resulting in increased water gradient for improved power generation (Fig. 4b). As shown in Fig. 4c, the generated current can maintain a value of ~22 μA under the solar irradiation, which can be effectively adjusted by a dynamic switch of simulated solar source. When the solar simulator equipped with AM 1.5G was applied, the generated voltage could have a controllable response to the solar irradiation and experience a remarkable improvement from ~0.47 V to ~0.6 V (Fig. 4d). It is noted that a continuous current signal output can still be observed with the current of ~6 μA even after 6 h (Fig. 4c).

Specifically, the simulated seawater with NaCl concentration of 3.5 wt% was employed in our system. However, it is considered that the ion concentration may significantly affect the resistance in the integrated system. Therefore, NaCl solution with a series of ion concentration of 3.5, 7 and 10.5 wt% was used to investigate the saturated current. As shown in Fig. S12, the saturated current can have a prominent improvement ranging from ~7.5 to ~12.7 μA. The result clearly illustrates that the increased NaCl concentration can remarkably reduce the resistance of the single electrode system and increase the corresponding saturated current, which can be effectively tuned through the adjustment of ion concentration. Additionally, the occupied area of PDMS is also one of the important factors during the power generation. As displayed in Fig. S13, the average weight content of PDMS is 38.87% in our system, in which the area ratio of paper and PDMS coating is about 1:1. Since the occupied area of PDMS on paper surface can significantly affect the performance of electricity production, samples with a series of PDMS area ratio were employed to conduct the experiments of power generation. As shown in Fig. S14, P is defined as the area ratio of PDMS and the whole paper, in which 0.25, 0.5 and 0.75 are used to explore the difference of corresponding electricity generation. It can be observed that when the P value is lower than 0.5, more PDMS area results in higher induced voltage. However, no remarkable increase of saturated voltage can be found under the circumstance of excess PDMS coating area with the P value of more than 0.5. The result may derive from the confined transportation distance of the water molecules. As a result, the area ratio of 0.5 is employed in our experiment.

In addition, the sketch of equivalent circuits were also displayed in Fig. 4e to illustrate the difference between single electrode and double electrodes system. It is noted that single electrode and double electrodes applied on CPPH surface are referred to single system and double system, respectively. In our experiments, the calculated resistance of single resistance value of the CPPH was similar to that of the double electrodes system (Fig. 4f). Therefore, it is supposed that the equivalent circuit can be further applied in our system. In addition, we have also conducted the control experiments of single electrode and double electrodes system. As shown in Fig. S15, the saturated voltage of single and double electrodes-based electricity generator demonstrates ~0.34 V and 0.11 V, respectively. Whereas, the output saturated current of double electrodes can reach up to ~47 μA, which is about 10 times larger than that of the single electrode system without sunlight irradiation. Note that the difference in output current and voltage between single and double electrode system is relatively complex due to the unidentified factors such as changeable contact resistance in the double electrode system. The

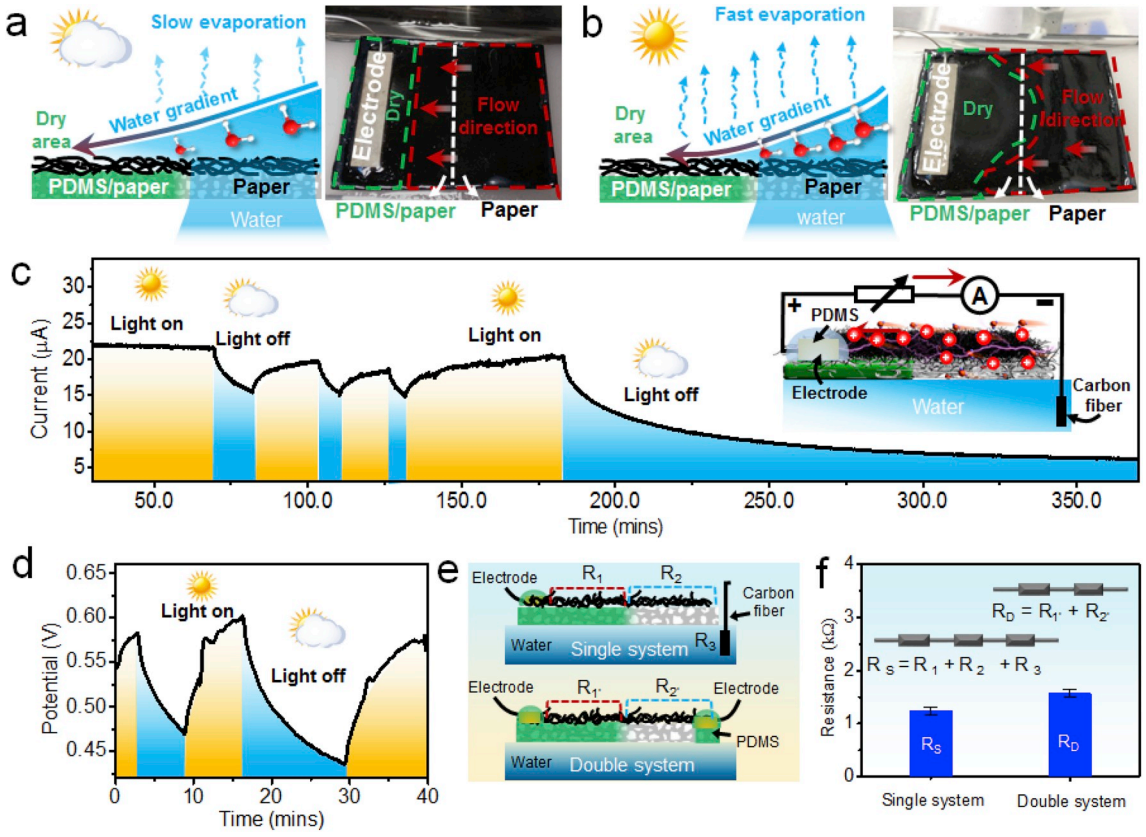

Fig. 4. Schematic illustration and photos of the water flow induced electricity generation without solar illumination a) and under 1 sun b). Real-time current c) and voltage collection d) with and without solar irradiation. e) Schematic of equivalent circuits, including single electrode system and double electrodes system applied on CPPH surface. f) Resistance column of single electrode and double electrodes system.

potential interface failure between hydrophilic CNTs film on paper side and applied electrode may experience unstable induced electricity generation. As a result, single electrode system is preferred in our system. However, further detailed mechanism will be systematically studied in future work.

Furthermore, for the combined evaporation and electricity generation applications, we have also compared our work with other related references, such as combined thermoelectric devices and salinity gradient-induced generators [27,40–42,64]. The abovementioned works have focused on the development of multifunctional devices with integrated clean water and electricity production. Based on the mechanism of water flow and evaporation, the solar-enhanced evaporator/-power generator enables comparative water evaporation rate and highest saturated voltage under 1 sun irradiation (Fig. S16).

Moreover, the output performance of the CPPH was further investigated by connecting external loads with various resistances. With the step-by-step decrease of the load resistance (0.9 MΩ–0.3 MΩ), the output current increased correspondingly (Fig. 5a). Moreover, when the load resistance increased from 1 Ω to 1 GΩ, the current on the load resistance decreased from ~22 μA to ~0 μA and the generated voltage increased from ~0 V to ~0.55 V (Fig. 5b). Meanwhile, with the adjustment of load resistance, the output power can experience a parabola tendency. The maximum output power can reach up to 2.1 μW (Fig. 5c). As a proof of concept, our system was employed as a power supply to drive a raindrop detector for monitoring the water droplets, which was schematically shown in Fig. 5d. In our experiment, the integrated CPPH floated on the simulated seawater surface was applied to power the raindrop sensor for a self-powering system. The detailed circuit diagram and corresponding picture of the integrated system were also displayed in Fig. 5e. Since the CPPH was connected to the detector, a real-time detection could be successfully realized. The current can respond sensitively to the water droplets with different frequencies, demonstrating great potentials in self-powering platforms (Fig. 5f). However, there are still some problems to be considered in the current proof-of-concept paper-based materials, such as the potential threats of salts aggregates, the durability of paper-based materials, *etc*. In our system, it is of significant concern to explore of water flow and evaporation process in an interface-confined system through asymmetric functionalization. As a cost-effective and scalable, portable and accessible alternative, the paper hybrid has still represented some specific advantages on the filed of convenient and disposable devices. Based on this strategy, specially treated papers and a variety of water-pumping substrates can be employed to realize the synergetic multifunctional applications, in which the abovementioned issues are expected to be effectively solved.

4. Conclusions

In summary, the process of water evaporation in the nature has enlightened us to exploit the significant potentials of water flow and evaporation. We demonstrate a concept of asymmetric functionalization strategy for multifunctional photo-thermal cellulose papers towards integrated clean water and power production. Through a capillarity driven transfer strategy, the self-assembled CNTs film at air/water interface can be unidirectionally transferred onto the paper surface with homogenous morphology and controllable thickness. The as-prepared CNTs/paper enables good flexibility, foldability and stability, which can function as the solar absorber for clean water collection. Moreover, when it was further asymmetrically decorated with hydrophobic PDMS layer on specific location of the paper side, a controllable pathway of water flow could be achieved. The resulted directional water flow enables efficient electricity generation, which can be further enhanced

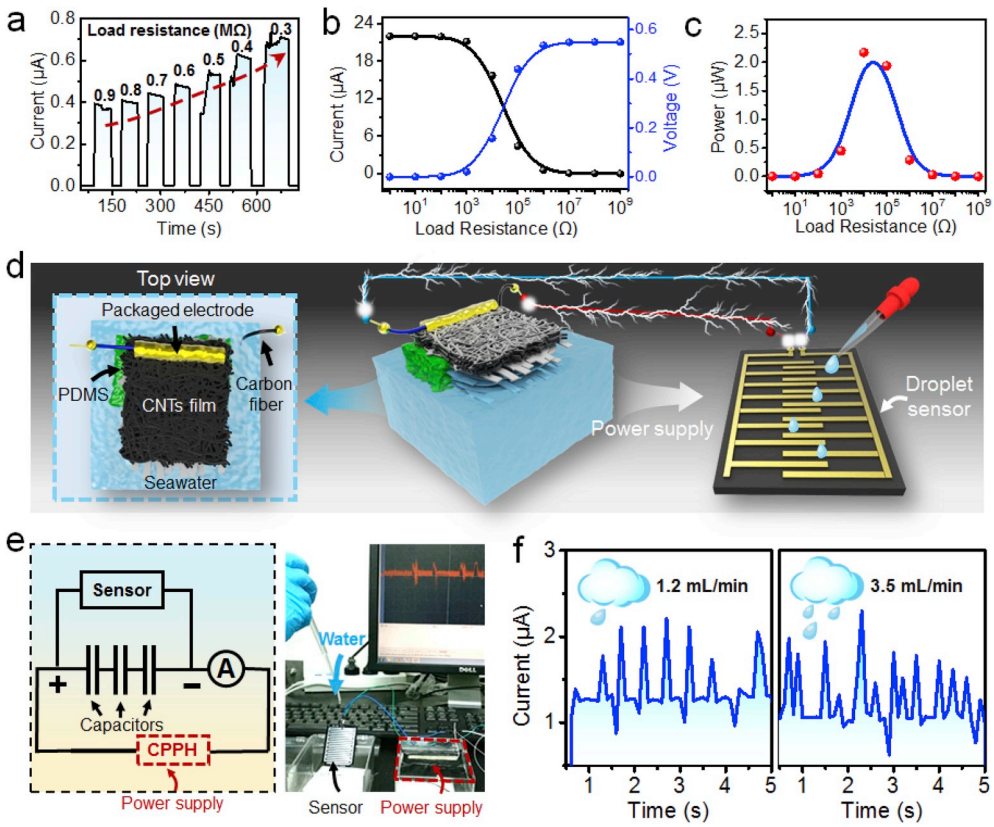

Fig. 5. a) The output current with different load resistance. The current and voltage on the load resistance b) and output power c) values can be effectively adjusted with a broad range. d) A schematic demo of self-powering sensor. e) Sketch and photograph of the device to detect the water droplet using the hybrid film as power supply. f) Real-time detecting water droplet with slow and fast velocity.

under sunlight illumination.

Declaration of competing interest

The authors declare that they have no known competing financial interests or personal relationships that could have appeared to influence the work reported in this paper.

Acknowledgements

P.X. and J.H. contributed equally to this work. We thank the Natural Science Foundation of China (51803226, 51573203), Key Research Program of Frontier Sciences, Chinese Academy of Sciences (QYZDB-SSW-SLH036), Postdoctoral Innovation Talent Support Program (BX20180321), China Postdoctoral Science Foundation (2018M630695) and Ningbo Science and Technology Bureau (2018A610108).

Appendix A. Supplementary data

Supplementary data to this article can be found online at https://doi.org/10.1016/j.nanoen.2019.104385.

References

[1] G. Xue, Y. Xu, T. Ding, J. Li, J. Yin, W. Fei, Y. Cao, J. Yu, L. Yuan, L. Gong, J. Chen, S. Deng, J. Zhou, W. Guo, Nat. Nanotechnol. 12 (2017) 317–321.
[2] H. Ghasemi, G. Ni, A.M. Marconnet, J. Loomis, S. Yerci, N. Miljkovic, G. Chen, Nat. Commun. 5 (2014) 4449.
[3] N.S. Lewis, Science 315 (2007) 798–801.
[4] H.M. Qiblawey, F. Banat, Desalination 220 (2008) 633–644.
[5] M.A. Shannon, P.W. Bohn, M. Elimelech, J.G. Georgiadis, B.J. Marinas, A. M. Mayes, Nature 452 (2008) 301–310.
[6] M.M. Gao, L.L. Zhu, C.K. Peh, G.W. Ho, Energy Environ. Sci. 12 (2019) 841–864.
[7] W. Liu, Z. Wang, G. Wang, G. Liu, J. Chen, X. Pu, Y. Xi, X. Wang, H. Guo, C. Hu, Z. L. Wang, Nat. Commun. 10 (2019) 1426.
[8] Q. Tang, M.-H. Yeh, G. Liu, S. Li, J. Chen, Y. Bai, L. Feng, M. Lai, K.-C. Ho, H. Guo, C. Hu, Nano Energy 47 (2018) 74–80.
[9] Q. Tang, X. Pu, Q. Zeng, H. Yang, J. Li, Y. Wu, H. Guo, Z. Huang, C. Hu, Nano Energy 66 (2019) 104087.
[10] L.A. Weinstein, J. Loomis, B. Bhatia, D.M. Bierman, E.N. Wang, G. Chen, Chem. Rev. 115 (2015) 12797–12838.
[11] S. Chu, Y. Cui, N. Liu, Nat. Mater. 16 (2017) 16–22.
[12] M.S. Dresselhaus, I.L. Thomas, Nature 414 (2001) 332–337.
[13] F. Bonaccorso, L. Colombo, G. Yu, M. Stoller, V. Tozzini, A.C. Ferrari, R.S. Ruoff, V. Pellegrini, Science 347 (2015) 1246501.
[14] A.J. Nozik, J. Miller, Chem. Rev. 110 (2010) 6443–6445.
[15] G. Williams, B. Seger, P.V. Kamat, ACS Nano 2 (2008) 1487–1491.
[16] W. Tu, Y. Zhou, Z. Zou, Adv. Mater. 26 (2014) 4607–4626.
[17] O. Neumann, A.S. Urban, J. Day, S. Lal, P. Nordlander, N.J. Halas, ACS Nano 7 (2013) 42–49.
[18] C.J. Chen, Y.D. Kuang, L.B. Hu, Joule 3 (2019) 683–718.
[19] F. Yi, H.Y. Ren, K.R. Dai, X.F. Wang, Y.Z. Han, K.X. Wang, K. Li, B.L. Guan, J. Wang, M. Tang, J.Y. Shan, H. Yang, M.S. Zheng, Z. You, D. Wei, Z.F. Liu, Energy Environ. Sci. 11 (2018) 2016–2024.
[20] Y. Liu, S. Yu, R. Feng, A. Bernard, Y. Liu, Y. Zhang, H. Duan, W. Shang, P. Tao, C. Song, T. Deng, Adv. Mater. 27 (2015) 2768–2774.
[21] L. Zhang, B. Tang, J. Wu, R. Li, P. Wang, Adv. Mater. 27 (2015) 4889–4894.
[22] L. Zhou, Y. Tan, J. Wang, W. Xu, Y. Yuan, W. Cai, S. Zhu, J. Zhu, Nat. Photonics 10 (2016) 393–398.
[23] G. Ni, G. Li, S.V. Boriskina, H. Li, W. Yang, T. Zhang, G. Chen, Nat. Energ. 1 (2016) 16126.
[24] C.J. Chen, Y.J. Li, J.W. Song, Z. Yang, Y. Kuang, E. Hitz, C. Jia, A. Gong, F. Jiang, J. Y. Zhu, B. Yang, J. Xie, L.B. Hu, Adv. Mater. 29 (2017) 1701756.
[25] P.P. Zhang, J. Li, L.X. Lv, Y. Zhao, L.T. Qu, ACS Nano 11 (2017) 5087–5093.
[26] J.L. Li, M.H. Du, G.X. Lv, L. Zhou, X.Q. Li, L. Bertoluzzi, C.H. Liu, S.N. Zhu, J. Zhu, Adv. Mater. 30 (2018) 1805159.
[27] X.F. Zhang, W.Q. Gao, X.W. Su, F.L. Wang, B.S. Liu, J.J. Wang, H. Liu, Y.H. Sang, Nano Energy 48 (2018) 481–488.
[28] K. Liu, T.P. Ding, J. Li, Q. Chen, G.B. Xue, P.H. Yang, M. Xu, Z.L. Wang, J. Zhou, Adv. Energ. Mater. 8 (2018) 1702481.
[29] H.D. Liu, Z. Huang, K. Liu, X.J. Hu, J. Zhou, Adv. Energ. Mater. 9 (2019) 1900310.
[30] P. Tao, G. Ni, C.Y. Song, W. Shang, J.B. Wu, J. Zhu, G. Chen, T. Deng, Nat. Energy 3 (2018) 1031–1041.
[31] W. Shang, T. Deng, Nat. Energy 1 (2016) 16133.

[32] R.Y. Li, L.B. Zhang, L. Shi, P. Wang, ACS Nano 11 (2017) 3752–3759.
[33] N. Xu, X.Z. Hu, W.C. Xu, X.Q. Li, L. Zhou, S.N. Zhu, J. Zhu, Adv. Mater. 29 (2017) 1606762.
[34] L.L. Zhu, M.M. Gao, C.K.N. Peh, X.Q. Wang, G.W. Ho, Adv. Energ. Mater. 8 (2018) 1702149.
[35] Y. Yang, X. Yang, L. Fu, M. Zou, A. Cao, Y. Du, Q. Yuan, C.-H. Yan, ACS Energy Lett 3 (2018) 1165–1171.
[36] Y. Ito, Y. Tanabe, J. Han, T. Fujita, K. Tanigaki, M. Chen, Adv. Mater. 27 (2015) 4302–4307.
[37] T. Li, H. Liu, X.P. Zhao, G. Chen, J.Q. Dai, G. Pastel, C. Jia, C.J. Chen, E. Hitz, D. Siddhartha, R.G. Yang, L.B. Hu, Adv. Funct. Mater. 28 (2018) 1707134.
[38] H. Liu, C.J. Chen, G. Chen, Y.D. Kuang, X.P. Zhao, J.W. Song, C. Jia, X. Xu, E. Hitz, H. Xie, S. Wang, F. Jiang, T. Li, Y.J. Li, A. Gong, R.G. Yang, S. Das, L.B. Hu, Adv. Energ. Mater. 8 (2018) 1701616.
[39] F. Zhao, X. Zhou, Y. Shi, X. Qian, M. Alexander, X. Zhao, S. Mendez, R. Yang, L. Qu, G. Yu, Nat. Nanotechnol. 13 (2018) 489–495.
[40] P.H. Yang, K. Liu, Q. Chen, J. Li, J.J. Duan, G.B. Xue, Z.S. Xu, W.K. Xie, J. Zhou, Energy Environ. Sci. 10 (2017) 1923–1927.
[41] L.L. Zhu, T.P. Ding, M.M. Gao, C.K.N. Peh, G.W. Ho, Adv. Energ. Mater. 9 (2019) 1900250.
[42] L. Zong, M.J. Li, C.X. Li, Nano Energy 50 (2018) 308–315.
[43] X. Li, X. Min, J. Li, N. Xu, P. Zhu, B. Zhu, S. Zhu, J. Zhu, Joule (2018).
[44] W. Wang, Y. Shi, C. Zhang, S. Hong, L. Shi, J. Chang, R. Li, Y. Jin, C. Ong, S. Zhuo, P. Wang, Nat. Commun. 10 (2019) 3012.
[45] T.P. Ding, K. Liu, J. Li, G.B. Xue, Q. Chen, L. Huang, B. Hu, J. Zhou, Adv. Funct. Mater. 27 (2017) 1700551.
[46] Z.H. Zhang, X.M. Li, J. Yin, Y. Xu, W.W. Fei, M.M. Xue, Q. Wang, J.X. Zhou, W. L. Guo, Nat. Nanotechnol. 13 (2018) 1109–1119.
[47] J. Park, S. Song, C. Shin, Y. Yang, S.A.L. Weber, E. Sim, Y.S. Kim, Angew. Chem. Int. Ed. 57 (2018) 2091–2095.
[48] M. Li, L. Zong, W. Yang, X. Li, J. You, X. Wu, Z. Li, C. Li, Adv. Funct. Mater. 45 (2019) 1901798.
[49] K. Liu, P.H. Yang, S. Li, J. Li, T.P. Ding, G.B. Xue, Q. Chen, G. Feng, J. Zhou, Angew. Chem. Int. Ed. 55 (2016) 8003–8007.
[50] H.H. Cheng, Y.X. Huang, F. Zhao, C. Yang, P.P. Zhang, L. Jiang, G.Q. Shi, L.T. Qu, Energy Environ. Sci. 11 (2018) 2839–2845.
[51] F. Zhao, H. Cheng, Z. Zhang, L. Jiang, L. Qu, Adv. Mater. 27 (2015) 4351–4357.
[52] Y. Liang, F. Zhao, Z. Cheng, Y. Deng, Y. Xiao, H. Cheng, P. Zhang, Y. Huang, H. Shao, L. Qu, Energy Environ. Sci. 11 (2018) 1730–1735.
[53] T. Xu, X.T. Ding, Y.X. Huang, C.X. Shao, L. Song, X. Gao, Z.P. Zhang, L.T. Qu, Energy Environ. Sci. 12 (2019) 972–978.
[54] L.F. Cui, P.P. Zhang, Y.K. Xiao, Y. Liang, H.X. Liang, Z.H. Cheng, L.T. Qu, Adv. Mater. 30 (2018) 1706805.
[55] P. Xiao, J. Gu, C. Wan, S. Wang, J. He, J. Zhang, Y. Huang, S.-W. Kuo, T. Chen, Chem. Mater. 28 (2016) 7125–7133.
[56] P. Xiao, Y. Liang, J. He, L. Zhang, S. Wang, J. Gu, J. Zhang, Y. Huang, S.-W. Kuo, T. Chen, ACS Nano 13 (2019) 4368–4378.
[57] Y. Liang, J. Shi, P. Xiao, J. He, F. Ni, J. Zhang, Y. Huang, C.-F. Huang, T. Chen, Chem. Commun. 54 (2018) 12804–12807.
[58] S. Wang, P. Xiao, Y. Liang, J. Zhang, Y. Huang, S. Wu, S.-W. Kuo, T. Chen, J. Mater. Chem. C 6 (2018) 5140–5147.
[59] Y. Liang, P. Xiao, S. Wang, J. Shi, J. He, J. Zhang, Y. Huang, T. Chen, J. Mater. Chem. C 6 (2018) 6666–6671.
[60] P. Xiao, J. Gu, J. He, S. Wang, J. Zhang, Y. Huang, S.-W. Kuo, T. Chen, J. Mater. Chem. C 4 (2016) 9750–9755.
[61] P. Xiao, J. He, Y. Liang, C. Zhang, J. Gu, J. Zhang, Y. Huang, S.-W. Kuo, T. Chen, Solar RRL 3 (2019) 1900004.
[62] J. Li, K. Liu, G.B. Xue, T.P. Ding, P.H. Yang, Q. Chen, Y. Shen, S. Li, G. Feng, A. G. Shen, M. Xu, J. Zhou, Nano Energy 48 (2018) 211–216.
[63] R. Zhang, S. Wang, M.-H. Yeh, C. Pan, L. Lin, R. Yu, Y. Zhang, L. Zheng, Z. Jiao, Z. L. Wang, Adv. Mater. 27 (2015) 6482–6487.
[64] Y. Zhang, S.K. Ravi, S.C. Tan, Nano Energy 65 (2019) 104006.

Dr. Peng Xiao received his Ph.D. in polymer chemistry and physics from Ningbo Institute of Materials Technology and Engineering, Chinese Academy of Sciences in 2017, under the supervision of Prof. Tao Chen. After that he joint Tao Chen's group as a postdoctoral research fellow. His current research interest focuses on the macroscopic self-assembly of 1D and 2D of carbon-based nanomaterials into 2D ultrathin films at air/water interface and further interfacial asymmetric modification to explore their potential applications in actuators, sensors and solar-to-thermal conversion.

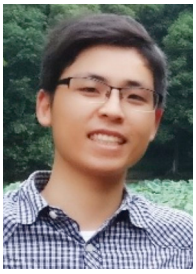

Dr. Jiang He received his M.S. degree from Ningbo University, China in 2016 under the supervision of Prof. Wenqin Wang from Ningbo University and Prof. Yousi Chen from Ningbo Institute of Materials Technology and Engineering, Chinese Academy of Sciences. After that, he got his Ph.D. in the Ningbo Institute of Materials Technology and Engineering, Chinese Academy of Sciences, under the supervision of Prof. Tao Chen. His research interests focus on the smart polymers and carbon nano materials hybrid with applications as actuators and sensors.

Feng Ni received his B.S. degree from Tianjin Polytechnic University in 2017. Currently, he is a PhD student in the Ningbo Institute of Materials Technology and Engineering, Chinese Academy of Sciences, under the supervision Professor Tao Chen. His current research interests focus on polymer/carbon-based 2D hybrid materials and photo-thermal conversion.

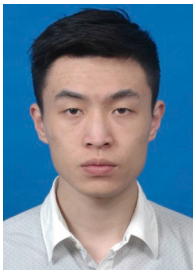

Chang Zhang received his B.S. degree from Ningbo Institute of Technology, Zhejiang University, China in 2016. Currently, he is a master candidate in the Ningbo University and the Ningbo Institute of Materials Technology and Engineering, Chinese Academy of Sciences, under the supervision of Prof. Wenqin Wang and Prof. Tao Chen. His research interests focus on the carbon-based hybrid materials toward application of photo-thermal conversion.

Yun Liang received his B.S. degree from Southwest University of Science and Technology. Currently, He is a PhD student in the Ningbo Institute of Materials Technology and Engineering, Chinese Academy of Sciences, under the supervision Professor Tao Chen and Youju Huang. His current research interests focus on polymer/Carbon-based 2D hybrid materials and their applications as sensors and actuators.

Wei Zhou received his B.S. degree from Harbin Engineering University in 2019. Now, he is a Ph.D. student in the Ningbo Institute of Materials Technology and Engineering, Chinese Academy of Sciences, under the supervision of Professor Tao Chen. His current research interests focus on the construction of carbon-based hybrid materials and their applications in self-powered sensors.

Jincui Gu received her MS degree in material science from Hainan University. In 2012, she joint Tao Chen's group as an assistant researcher. Her current research focuses on construction of the polymer functionalized carbon-based membranes for water purification.

Junyuan Xia received his B.S degree from Ningbo Institute of Technology, Zhejiang University. In 2018, he joint Tao Chen's group as an engineer. His current research focus on carbon-based membranes for waste water purification.

Prof. Shiao-Wei Kuo received his B.Sc. in chemical engineering from the National Chung Hsing University (1998) and Ph.D. in applied chemistry from the National Chiao Tung University in Taiwan (2002). He continued his research work at Chiao Tung University as a postdoctoral researcher during 2002–2007. Now, he is the professor in the Department of Materials and Optoelectronic Science, National Sun Yat-Sen University, Taiwan. His research interests include polymer interactions, self-assembly nanostructures, covalent organic frameworks, porous materials, POSS nanocomposites, polybenzoxazine, and polypeptides.

Prof. Tao Chen received his Ph.D. in polymer chemistry and physics from Zhejiang University in 2006. After his postdoctoral training at the University of Warwick (UK), he joined Duke University (USA) as a research scientist. He then moved back to Europe as an Alexander von Humboldt Research Fellow at Technische Universität Dresden, Germany. Since 2012, he is a full-time professor at Ningbo Institute of Materials Technology and Engineering, Chinese Academy of Sciences. His research interests include smart polymers and their hybrid systems with applications as actuators, shape memory polymers, and chemical sensing.